Chao et al. *Zool. Res.* 2026, 47(4): 1220−1234
https://doi.org/10.24272/j.issn.2095-8137.2025.288
https://cstr.cn/32248.14.zr.2025.288

ZR | Zoological Research

Article Open Access

Molecular mechanisms of the hypothalamus miR-27a/*PRKCA* pathway in regulating neuronal function and aggression-related behavior

Xiao-Huan Chao[1], Chun-Lei Zhang[1], Huan Yang[1], Qing-Lei Xu[1], Ming-Zheng Liu[1,2], Jia-Hao Chen[1], Shu-Han Liu[1], Zi-Ming Wang[1], Yuan Ding[1], Hong-Wei Bi[1], Wen Guo[1], Jun-Hong Fan[1], Meng-Jun Zhou[1], Jian-Sheng Ma[1], Asim Muhammad[1], Mubashir Muhammad[1], Bo Zhou[1,*]

[1] *College of Animal Science and Technology*, *Nanjing Agricultural University*, *Nanjing*, *Jiangsu* 210095, *China*

[2] *Faculty of Life Science and Technology*, *Kunming University of Science and Technology*, *Kunming*, *Yunnan* 650500, *China*

ABSTRACT

The intensification of livestock production has heightened public concern about animal welfare, with aggressive behavior recognized as a key determinant of both welfare and productivity. MicroRNAs (miRNAs), which are critical post-transcriptional regulators, have emerged as important modulators of animal behavior. This study investigated the molecular basis of aggression in pigs (*Sus scrofa*), focusing on miRNA-mediated regulation. Hypothalamic miRNA-sequencing of the most aggressive (*n*=4) and least aggressive (*n*=4) piglets identified nine differentially expressed miRNAs. Among these, miR-27a was significantly upregulated in aggressive individuals. Functional assays demonstrated that both porcine miR-27a and its human (*Homo sapiens*) ortholog has-miR-27a-3p, suppressed autophagy, apoptosis, and neuronal plasticity in primary porcine neurons and human SH-SY5Y neuroblastoma cells. To clarify the underlying mechanisms, mRNA-sequencing was performed on porcine neurons transfected with miR-27a mimics or negative controls, identifying 436 differentially expressed genes (84 upregulated and 352 downregulated). Gene Ontology (GO), Kyoto Encyclopedia of Genes and Genomes (KEGG), and protein-protein interaction (PPI) analyses highlighted eight genes—*CBL*, *PRKCA*, *SLC38A1*, *ZBTB16*, *AANAT*, *CYP1A1*, *SLC7A11*, and *NTRK2*—associated with tryptophan metabolism, oxidative stress, and long-term synaptic depression. Bioinformatic analysis and dual-luciferase reporter assays confirmed that miR-27a directly targets the 3′-UTR of *PRKCA*, thereby suppressing of autophagy, apoptosis, and neuronal plasticity. *In vivo*, intrahypothalamic injection of mmu-miR-27a-3p in mice (*Mus musculus*) reduced motor function and social dominance, and placed the mice at a competitive disadvantage, while supressing neuronal autophagy, apoptosis and plasticity.

Keywords: Pig; Aggressive behavior; Hypothalamus; miR-27a; *PRKCA*; SH-SY5Y cell line; Mouse

INTRODUCTION

Aggressive behavior in animals can lead to injury or death, thereby influencing individual fitness, population dynamics, and ecosystem stability (Tubert et al., 2012; van der Steen et al., 1988). Intensive pig farming frequently attains enhanced efficiency through the implementation of strategies such as relocation and group mixing. During this process, pigs engage in intense aggression to re-establish dominance hierarchies after regrouping. These confrontations often cause superficial injuries, reduced growth rates, and diminished meat quality, while compromising herd welfare and imposing substantial economic losses on producers (Galli et al., 2023; Wei et al., 2023).

Aggression is a complex social trait shaped throughout life by both internal and external factors, including genetics, nutrition, the environment, disease, and physiological state (Hage et al., 2009; Mikkola et al., 2021; Nieuwenhuis et al., 2022; Weltens et al., 2021; Zhang et al., 2025). For example, carbonated-beverageconsumption, high-fat diets, occupational noise, and environmental changes have been shown to affect aggression in humans and animal models (Alimohammadi et al., 2018; Burrows et al., 2020; Shi et al., 2020; Turner et al., 2008; Zilkha et al., 2024). Genetic mutations, specific single-nucleotide polymorphisms (SNPs), and copy-number variations (CNVs) can also substantially influence aggressiveness (Xu et al., 2022; Zhang et al., 2023).

MicroRNAs (miRNAs) are critical post-transcriptional regulators that orchestrate diverse physiological and

Received: 25 September 2025; Accepted: 10 November 2025; Online: 11 November 2025

Foundation items: This work was supported by the National Natural Science Foundation of China (32172786), and Independent Innovation Funds for Agricultural Science and Technology in Jiangsu Province (CX (24)1014)

*Corresponding author, E-mail: zhoubo@njau.edu.cn

pathological processes. Their effects on behavior has attracted growing attention, with evidence linking miRNAs to learning, memory, emotional regulation, stress adaptation, and aggression. For instance, hippocampal inhibition of miR-186-5p alleviates depression-like behavior, whereas elevated miR-132/212 levels in the amygdala are associated with increased anxiety (Aten et al., 2019; Jiang et al., 2021). Furthermore, a specific variant (rs3262221458) in the 3′-UTR of porcine *JARID2* regulates aggression by affecting miR-9828-3p binding, piglets with the TT genotype are more aggressive (Yang et al., 2024).

miR-27a has been implicated in a wide range of biological processes, including cell proliferation, apoptosis, inflammation, and metabolism (Li et al., 2019, 2022; Salerno et al., 2024). miR-27a-3p has been observed to target MAP2K4, thereby reducing inflammation and neuronal death in epilepsy (Lu et al., 2019). In athletes with concussion, plasma miR-27a levels are reduced and inversely correlated with injury severity, suggesting a neuroprotective role (Shultz et al., 2022). Moreover, miR-27a and its rs895819 polymorphism have been linked to bipolar affective disorder, with the C mutation in pre-miR-27a altering cell migration and dopamine expression (Yang et al., 2022).

Despite these findings, the role of miR-27a in aggression remains poorly understood. In this study, we performed hypothalamic miRNA-seq to identify miRNAs associated with aggression in pigs and demonstrated that miR-27a regulates autophagy, apoptosis, and neuronal plasticity in vitro. In vivo experiments further confirmed that miR-27a modulates aggressive behavior in mice. Collectively, these results provide novel insights into the molecular mechanisms underlying miRNA-mediated regulation of social behavior.

MATERIAL AND METHODS

Experimental animal management

Animal experiments were conducted in the nursery unit of a commercial pig farm (Jiangsu Huaduo Animal Husbandry Technology Co., Ltd., China). A total of 160 healthy weaned Large White pigs (28 days old; 8.39±0.78 kg) were blocked by body weight and allocated into eight pens (20 pigs per pen; 10 females and 10 barrows) of dimensions 4 m long×3 m wide. Pigs had ad libitum access to feed and water.

Behavior was continuously recorded for 48 h post-mixing using cameras (EZVIZ CB3, Hangzhou Ezviz Network, China). To facilitate individual identification, pigs were marked with unique spray-painted symbols on their backs. Aggressive behaviors were quantified by video analysis, recording the frequency and duration of active attacks, bullying, and stand-off behaviors.

A composite aggression score (CAS) was calculated as follows (Desire et al., 2016; Guo et al., 2022; Shen et al., 2020):

$$\text{CAS} = \text{frequency of active attacks} + 0.07 \times \text{duration of active attacks (s)} \quad (1)$$

From each pen, the five most aggressive and the five least aggressive pigs were selected for regrouping. During the second regrouping, the 40 most aggressive pigs selected after the first regrouping were allocated to two pens (20 pigs per pen), and the 40 least aggressive pigs were allocated to another two pens. Behavior was again recorded for 48 h after mixing. Based on CAS values, two highly aggressive and two minimally aggressive pigs were selected from each pen (n=8). CAS values are presented in Table 1.

At the end of the second regrouping, four of the most aggressive pigs and four of the least aggressive pigs were humanely euthanized. Tissues (pituitary gland, parietal lobe, and temporal lobe) were collected, flash-frozen in liquid nitrogen, and stored at –80°C. All procedures were approved by the Animal Care and Use Committee of Nanjing Agricultural University (Approval No. NJAULLSC2021030).

Total RNA extraction and miRNA-seq

Total RNA was extracted using TriQuick Reagent (SolarBio, China) according to the manufacturer's protocol. Briefly, approximately one mung bean-sized tissue piece was homogenized in 750 μL TriQuick, followed by phase separation with chloroform (150 μL; Damao, China). RNA was precipitated with an equal volume of isopropanol (Damao, China), washed with 75% ethanol, and dissolved in 25 μL of RNase-free water (SolarBio, China).

RNA samples were sequenced at Biomarker Technologies (China). Raw reads were quality-checked with FastQC, trimmed with Trimmomatic, and aligned to the pig reference genome using Bowtie or STAR. Known miRNAs were annotated via miRBase, and expression was normalized as transcripts per million (TPM). Differentially expressed miRNAs (DEMs) were identified using DESeq2 (v.0.3.1) with thresholds $|\log_2(\text{fold change})| \geq 0.75$ and P-value<0.05. Volcano plots and heatmaps were generated using http://www.bioinformatics.com.cn/. Correlations between DEMs and CAS were assessed by Pearson correlation analysis.

mRNA-seq and differential screening of genes

Total RNA was sequenced at Biomarker Technologies (China) using the NEBNext Ultra RNA Library Prep Kit (NEB, USA) and an Illumina NovaSeq 6000 platform (PE150, USA). Approximately 6 GB of data were obtained per sample. Clean

Table 1 Composite aggression scores of the eight experimental pigs

Pig ID	Weight（kg)	Frequency of active attacks	Duration of active attacks time (s)	Composite aggression score (CAS)*
M1	9.75	14	270	32.9
M2	9.55	10	228	25.96
M3	8.65	20	348	44.36
M4	8.65	16	296	36.72
Mean±SD	9.15±0.51	15±3.61**	285.5±43.48**	34.985±6.65**
L1	10	2	32	4.24
L2	9.2	5	48	8.36
L3	8.3	2	16	3.12
L4	8.95	1	7	1.49
Mean±SD	9.11±0.61	2.5±1.5	25.75±15.66	4.3025±2.54
P-value	0.9372	0.0012	0.0001	0.0003

reads were mapped to the pig reference genome (Sscrofa 11.1; http://asia.ensembl.org/Sus_scrofa/Info/Index) using HISAT2 (v.2.0.5), and gene counts were generated with featureCounts (Subread v.2.0.1). To capture genes indirectly regulated by miRNAs or showing modest expression changes, differentially expressed genes (DEGs) were identified using DESeq2 (v.0.3.1) with thresholds of $|\log\log_2(\text{fold change})| \geq 0.6$ and *P*-value<0.05. Functional enrichment analyses, including Gene Ontology (GO) and Kyoto Encyclopedia of Genes and Genomes (KEGG) analyses, were performed using KOBAS (http://bioinfo.org/kobas). Gene set enrichment analysis (GSEA) was conducted using the same platform.

Reverse Transcription quantitative Polymerase Chain Reaction (RT-qPCR)

RNA quantification was followed by cDNA synthesis using One-Step RT-gDNA Digestion SuperMix for qPCR (Yeasen, China). For miRNA reverse transcription, the SuperStar miRNA First-Strand cDNA Synthesis Kit (tailing A method, Cowin Biotech, China) was used. qPCR was performed using Universal Blue qPCR SYBR Green Master Mix (Yeasen, China). Primers were designed using NCBI Primer-BLAST and verified via BLAST. Sequences are listed in Supplementary Table S1.

Isolation and culture of primary porcine neurons

Thirty-day-old weaned piglets were anesthetized with intranasal ether inhalation and euthanized by cardiac exsanguination. Brains were excised, washed in PBS (Biosharp, China), and transferred to pre-cooled D-Hanks' balanced salt solution (Biosharp, China). Tissue was digested in papain (2 mg/mL, Merck, Germany) and DNase I (10 mg/mL, Beyotime, China) at a 6:1 ratio. Equal volumes of the enzyme mixture and brain tissue were combined, and the tissue was minced into ~1 mm^3 fragments. An additional equal volume of enzyme solution was added, and the mixture was incubated at 37°C for 30 min.

Digestion was stopped with DMEM/F12 medium (Gibco, USA) supplemented with 10% fetal bovine serum (FBS, Gibco, USA). Suspensions were gently triturated and filtered (40 μm), centrifuged (1 000 r/min, 10 min), and washed three times in PBS at room temperature. Finally, cells were resuspended in complete DMEM/F12 medium containing 10% FBS and seeded into poly-L-lysine–coated T25 flasks. Cells were maintained at 37°C in a 5% CO_2 incubator. After 24 h, the medium was replaced. When cell confluence reached ~80%, cells were passaged for subsequent identification and transfection (Supplementary Figure S1).

Cell culture and cell transfection

Frozen cell vials were rapidly thawed in a 37°C water bath and mixed with an equal volume of complete medium containing 10% FBS. The suspension was centrifuged at 1 000 r/min for 5 min, the supernatant discarded, and the pellet resuspended in fresh complete medium. Cells were transferred to flasks containing 4–5 mL of complete medium and incubated at 37°C with 5% CO_2. SH-SY5Y cells were cultured in DMEM/F12 (Gibco, USA) supplemented with 10% FBS, while HEK 293T cells were maintained in high-glucose DMEM (Gibco, USA) with 10% FBS. Cell transfections were performed using Lipofectamine 3000 (Invitrogen, USA) following the manufacturer's protocol. After 48 h post-transfection, adherent cells were gently detached using 0.25% EDTA-trypsin solution (Gibco, USA). Cells were collected by centrifugation at 1 000 r/min for 5 min, washed with PBS, and resuspended to form a single-cell suspension. Following a second centrifugation step, the resulting cell pellet was stained according to the manufacturer's protocol using the Annexin V-FITC/PI Apoptosis Detection Kit (Vazyme, China). Apoptosis was immediately assessed using a CytoFlex flow cytometer (Beckman, USA).

Western blotting

Total protein was extracted using RIPA lysis buffer on ice. Protein samples were separated by electrophoresis on a 12% SDS-PAGE gel (EpiZyme, China) at 120 V for 60 min and transferred to PVDF membranes (Bio-Rad, USA) using a constant current of 330 mA. Membranes were blocked with Western Blocking Buffer (Beyotime, China) at room temperature for 1 h and then washed three times with TBST. Membranes were segmented based on the molecular weights of target proteins and incubated overnight at 4°C with the following primary antibodies: BCL2 (1:1 000, CY6717, Abways), ATG5 (1:1 000, ab108327, Abcam, UK), SynCAM (1:1 000, AY1462, Abways, China), Caspase-3 (1:1 000, A2156, ABclonal, China), PSD95 (1:1 000, CY5407, Abways, China), p62 (1:1 000, 18420-1-AP, Proteintech, USA), Tubulin (1:4 000, ab7291, Abcam, UK), and GAPDH (1:5 000, AF7021, Affinity, China). After three TBST washes, membranes were incubated with HRP-conjugated anti-rabbit IgG secondary antibody at room temperature for 1 h, followed by three additional washes with TBST. Protein bands were visualized using a high-sensitivity ECL chemiluminescence kit and imaged with the ChemiDoc XRS+system (Bio-Rad, USA). Band intensities were quantified using ImageJ software.

Flow cytometry

After 48 h of transfection, adherent cells were gently detached using 0.25% EDTA-pancreatin (Gibco, USA). Cells were collected by centrifugation at 1 000 r/min for 5 min, washed with PBS, and resuspended as a single-cell suspension. After a second centrifugation, the cell pellet was stained with an Annexin V-FITC/PI Apoptosis Detection Kit (Vazyme, China) according to the manufacturer's instructions. Apoptosis was immediately assessed using a CytoFlex flow cytometer (Beckman Coulter, USA).

TUNEL assay

Cells were seeded onto culture plates containing glass slides. When the cell density reached 75%–80%, transfection was initiated. After 48 h, apoptosis was assessed using TUNEL staining. Cells were fixed with 4% paraformaldehyde for 30–60 min and washed three times with PBS. Permeabilization was performed by incubating the cells in 0.1% Triton X-100 in PBS for 15 min at room temperature, followed by three PBS washes. Staining was carried out according to the manufacturer's instructions using the TUNEL Apoptosis Detection Kit (Yeasen, China). Images were captured and analyzed using a confocal microscope (Leica Microsystems, Wetzlar, Germany).

Multiplex immunofluorescence

Tissues or cells were fixed with 4% paraformaldehyde (Beyotime, China) and processed into sections. Membrane permeabilization was achieved using 0.3% Triton X-100 (Beyotime, China), followed by three PBS washes. Endogenous peroxidase activity was quenched by incubation with 3% H_2O_2 (Merck, Germany) for 10–15 min at room temperature, followed by PBS washes. Sections were blocked with 5% BSA at room temperature for 30 min. Primary antibodies, diluted appropriately, were applied and incubated

at 4°C for 2 h, followed by three PBS washes. Fluorescently labeled secondary antibodies, specific to the host species of the primary antibodies, were applied for 50 min at room temperature, followed by three additional PBS washes.

TYR-520 fluorescent dye (Abclonal, China) was mixed with TSA buffer and incubated for 5–10 min at room temperature, then washed with PBS. Elution was carried out at 37°C. These steps were repeated for the subsequent antibodies. After the final target antibody was applied, sections were stained with DAPI (Beyotime, China) for 10 min in the dark, washed with PBS, and mounted with an antifade reagent. Images were acquired using a confocal microscope (Leica Microsystems, Wetzlar, Germany).

The primary antibodies used were p62 (AFRM9025, AiFang Biological, 1:500, China), BCL2 (AFRM9319, AiFang Biological, 1:500, China), Bax (AFRM9175, AiFang Biological, 1:500, China), BAX (AFRM9175, AiFang Biological, 1:500, China), LC3B (AB48394, AiFang Biological, 1:400, China), NEFH (AF301083, AiFang Biological, 1:700, China), MBP (AF20147, AiFang Biological, 1:600, China).

Plasmid construction and oligonucleotide synthesis

The wild-type (WT) and mutant (Mut) plasmids containing the 3′-UTR of *PRKCA* were synthesized by Genecreate (China). The full coding sequence (CDS) of *PRKCA* (XM_021066740.1) was synthesized by White Whale Biotechnology (China) and cloned into the pcDNA3.1 vector, designated as *PRKCA*-pcDNA3.1. miR-27a mimics, inhibitors, negative controls (NC), agomir-miR-27a-3p, agomir-miR-27a-3p-NC, and PRKCA siRNA were synthesized by Generay (China). The agomir-miR-27a-3p was designated as miR-27a-3p-mimics, and the agomir-miR-27a-3p-NC as miR-27a-3p-mimic-NC. The siRNA targeting *PRKCA* was referred to as si-*PRKCA*. The sequences of all oligonucleotides are listed in Supplementary Table S2.

Target prediction and dual-luciferase reporter assay

Potential target genes of miR-27a were predicted by analyzing the 3′-UTR regions of downregulated differentially expressed genes using RNAhybrid (https://bibiserv.cebitec.uni-bielefeld.de/rnahybrid/submission.html/). For experimental validation, WT and Mut 3′-UTR constructs of *PRKCA* were co-transfected with miR-27a mimics or negative controls into 293T cells. After 36 h, the medium was removed and the cells were washed with PBS. Luciferase activity was measured using the Dual-Luciferase Reporter Assay Kit (Vazyme, China), following the manufacturer's protocol.

Hypothalamic injection of miR-27a-3p mimics and control

Based on the murine developmental timeline, weaning occurs at three weeks of age. Informed by prior pig group-mixing experiments and mouse developmental stages, male C57 mice were selected for this study. After 21 days of housing, mice were individually identified with ear tags. One week later, bilateral hypothalamic injections of miR-27a-3p-mimics or miR-27a-3p-mimic-NC were performed, delivering 1.5 nmol/μL per mouse. Body weights of the mice are provided in Supplementary Table S3. Throughout the experiment, animals were housed in a quiet environment with ad libitum access to food and water, and the room temperature was maintained at 25±2°C.

Behavioral tests

Behavioral assessments were conducted two days after hypothalamic injection of miR-27a-3p-mimics or miR-27a-3p-mimic-NC. In the open field test, mice were placed individually into the testing arena, and their movements were video-recorded. Behavioral data were analyzed using a video tracking system from Xinxin Information Technology (China). The total time spent in the testing area, the total distance moved, and the time spent in the central area were used to assess the level of anxiety exhibited by the subjects.

In the tube test, one mouse from the mimic group and one from the control group were placed at opposite ends of a tube. When the mice met in the center, the partition was removed to initiate confrontation. The test continued until one mouse retreated, indicating defeat (Noh et al., 2023). Each mouse in the mimic group was paired with each mouse in the control group. Competitiveness and social dominance were evaluated from the proportion of tube-test trials won by each mouse (Zhou et al., 2017). In the warm-spot test, two mice from each group were placed in a test arena. The time that each mouse occupied a prewarmed spot during a 5 min trial was recorded and used to assess social rank and competitive ability (Coleman et al., 2024).

Nissl staining

Paraffin-embedded brain sections were dewaxed and stained with 1% hematoxylin solution (Merck, Germany) for 30 min. After washing with distilled water, sections underwent color differentiation in 70% ethanol (J&K Scientific, China) for 30 s. Samples were sequentially dehydrated in 70%, 80%, and 95% ethanol (2 min each), followed by two 5 min immersions in absolute ethanol and two 10 min immersions in xylene. Sections were mounted using DPX Mountant (HEDE BIOTECHNOLOGY, China) and examined microscopically.

Statistical analysis

Pearson correlation coefficients were calculated to assess associations between miRNA expression and CAS. Western blotting data were normalized before analysis. Statistical significance was assessed using a *t*-test. Differences were considered statistically significant at $P<0.05$. Data are presented as the mean±standard error of the mean (SEM).

RESULTS

miR-27a regulates autophagy, apoptosis, and neuronal plasticity in primary porcine nerve cells

To investigate the molecular basis of aggressive behavior in pigs, hypothalamic tissues from the most and least aggressive pigs were subjected to miRNA-sequencing. Using thresholds of $|\log_2(\text{fold change})|\geq 0.75$ and P-value < 0.05, nine differentially expressed miRNAs were identified, eight were downregulated and one was upregulated (Figure 1A, B). Correlation analysis of miRNA transcripts per million (TPM) values and CAS values showed that ssc-miR-27a was the only miRNA significantly and positively correlated with aggression ($R=0.73$, $P=0.038$; Figure 1C). qPCR confirmed that miR-27a was significantly upregulated in the most aggressive group, consistent with the sequencing results (Figure 1D). To examine the functional role of miR-27a, we isolated primary neurons from porcine brain tissue and confirmed their identity and purity by immunofluorescence (Supplementary Figure S1). Because regrouping induces psychosocial stress, which can modulate cellular autophagy, apoptosis, and neuronal plasticity, we investigated the effects of miR-27a on these processes. Transfection of primary neurons with a miR-27a mimic or inhibitor (Figure 1E, F) showed that the mimics significantly reduced ATG5 mRNA and protein levels. It also significantly increased p62 mRNA

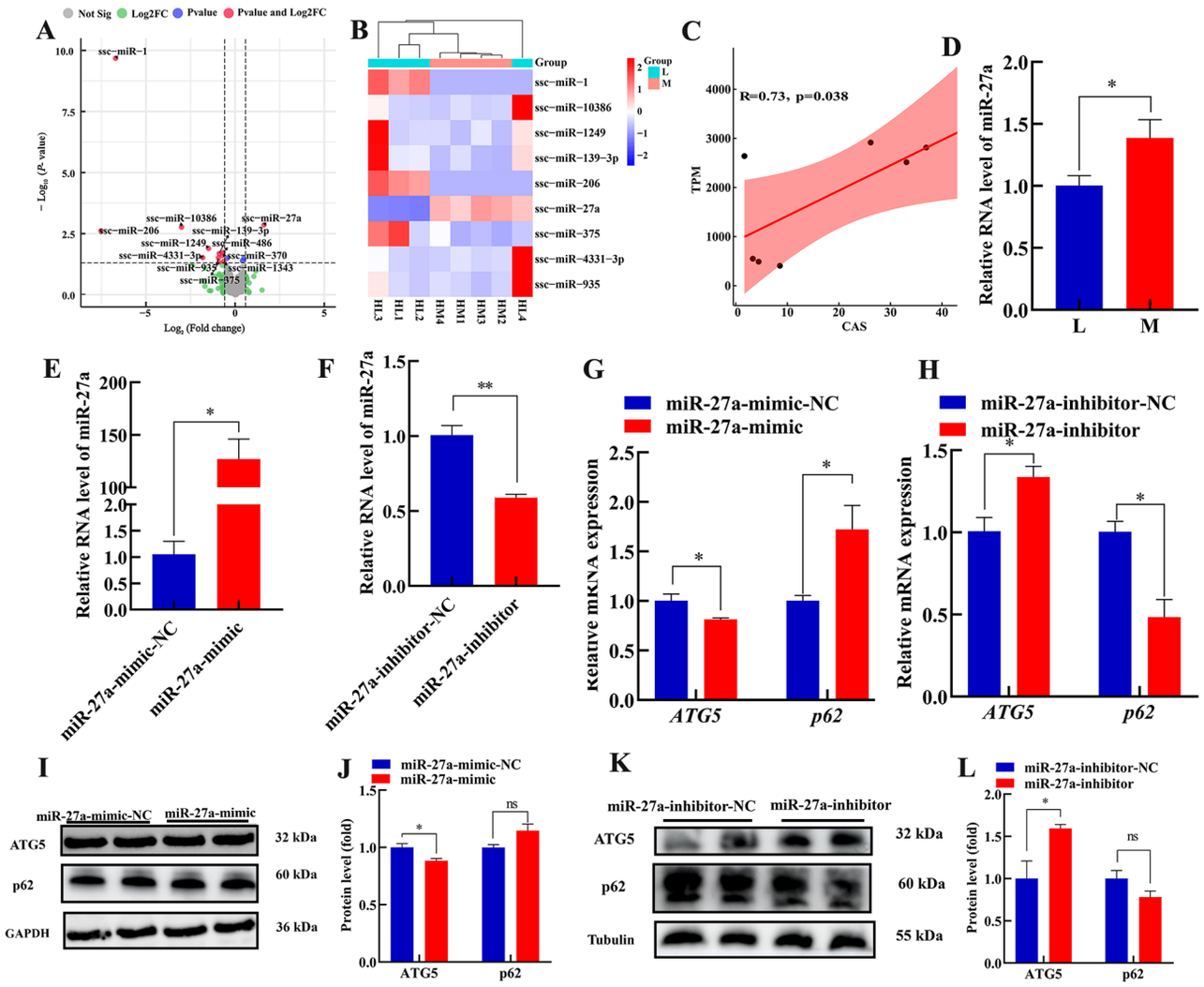

Figure 1 miR-27a is upregulated in the hypothalamus of aggressive pigs and inhibits autophagy in primary porcine neurons

A, B: Volcano plot and hierarchical clustering heatmap showing differentially expressed miRNAs in the hypothalamus of the most aggressive (HM) and least aggressive (HL) pigs. C: Correlation analysis between ssc-miR-27a expression (TPM values) and the composite aggression score (CAS). D: qPCR verification of miR-27a expression in the hypothalamic tissues of the least-aggression group (L) and the most-aggression group (M). E, F: Transfection efficiency of miR-27a mimics and inhibitors in primary porcine nerve cells, assessed by RT-qPCR. G, H: Relative mRNA expression levels of *ATG5* and *p62* following miR-27a mimic or inhibitor transfection. I, J: Western blot analysis of ATG5 and p62 protein expression in neurons transfected with miR-27a mimics (n=3). K, L: Western blot analysis of ATG5 and p62 protein expression in neurons transfected with miR-27a inhibitors (n=3). Data are presented as mean±SEM. *: P<0.05; **: P<0.01; ns: Not significant.

levels, although the increase in p62 protein levels was not significant (Figure 1G, I, J). Conversely, miR-27a inhibition led to increased ATG5 expression and decreased p62 expression at both the transcript and protein levels (Figure 1H, K, L). These results suggest that miR-27a suppresses autophagy.

Apoptosis-related analyses showed that miR-27a mimics significantly increased the *BCL2*/*Bax* mRNA ratio and reduced expression of *Caspase-1*, *Caspase-3*, and *Caspase-7* (Figure 2A). Opposite trends were observed following miR-27a inhibition (Figure 2B). Western blot analysis confirmed that miR-27a mimics decreased Caspase-3 protein levels, while the inhibitor increased them (Figure 2C, D). Flow cytometry further confirmed that miR-27a reduced neuronal apoptosis, whereas its inhibition promoted it (Figure 2E, F). Regarding neuronal plasticity, miR-27a mimics significantly decreased the mRNA expression of *SynCAM* and *PSD95*, both key markers of synaptic integrity. The expression of SynCAM at the protein level showed the same trend. In contrast, miR-27a inhibition upregulated their expression (Figure 2G–I). Collectively, these findings demonstrate that miR-27a is involved in autophagy, apoptosis, and neuronal plasticity in primary porcine neurons, suggesting a mechanistic link between miR-27a expression and stress-induced neurobehavioral adaptation.

miR-27a-3p modulates autophagy, apoptosis, and plasticity in the SH-SY5Y cell line

MicroRNA sequences are highly conserved across species. Sequence alignment showed that porcine ssc-miR-27a is identical to the human hsa-miR-27a-3p (Figure 3A). To investigate the role of miR-27a-3p in human neuronal cells, we performed functional assays in SH-SY5Y neuroblastoma cells. Transfection with miR-27a-3p mimics significantly suppressed *ATG5* and *LC3B* mRNA expression and increased p62 expression (Figure 3B, C). Conversely, a miR-27a-3p inhibitor enhanced *ATG5* and *LC3B* expression and reduced *p62* expression (Figure 3D). At the protein level, the mimics significantly decreased ATG5 and increased p62 expression (Figure 3E). The inhibitor only significantly increased p62

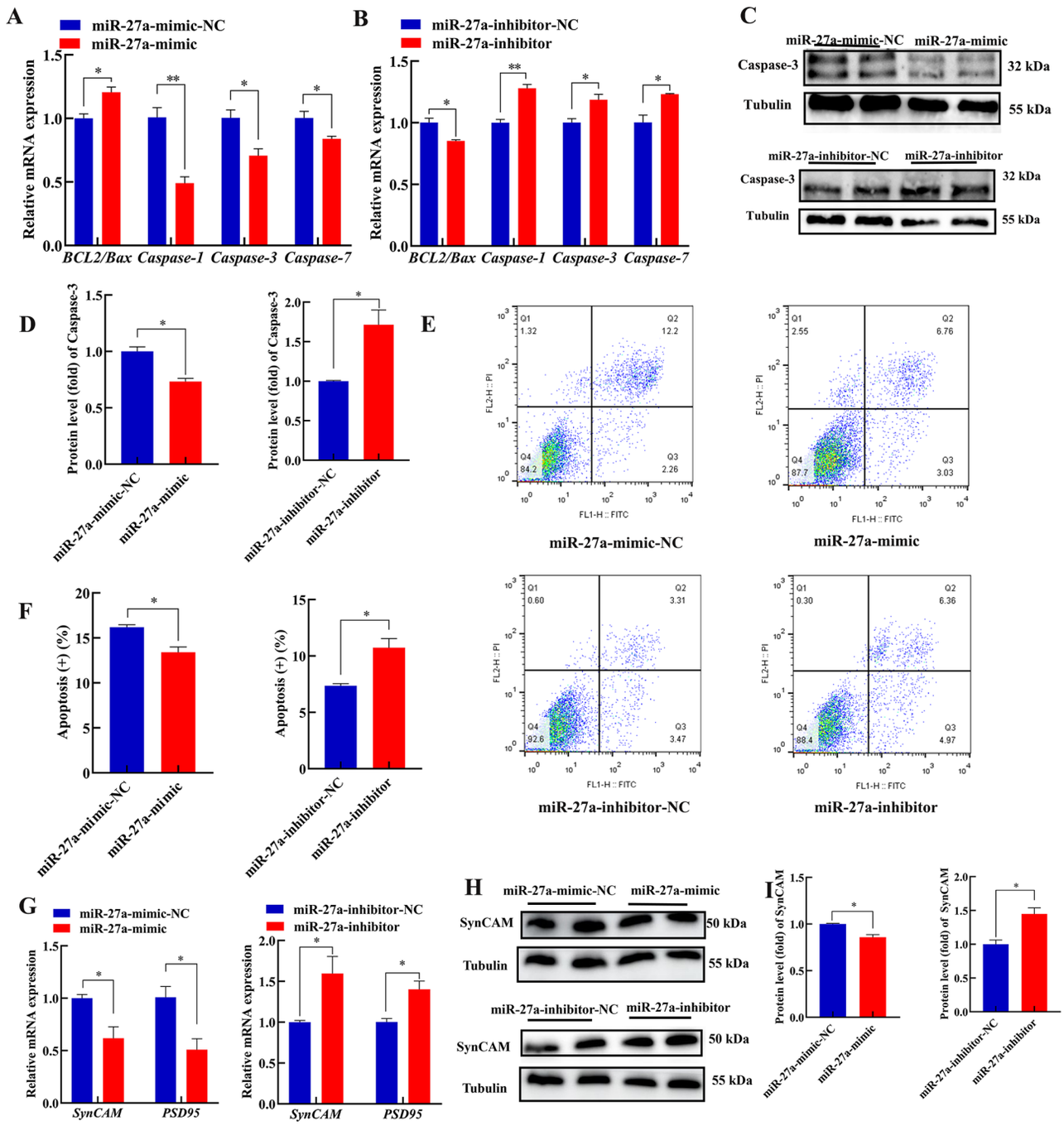

Figure 2 miR-27a inhibits apoptosis and neuronal plasticity in primary porcine nerve cells

A–B: Relative mRNA expression levels of apoptosis-related genes (*BCL2*, *Bax*, *Caspase-1*, *Caspase-3*, and *Caspase-7*) following transfection with miR-27a mimics or inhibitors. C–D: Western blot analysis of Caspase-3 protein expression in neurons transfected with miR-27a mimics or inhibitors (n≥3). E–F: Flow cytometry analysis showing the proportion of apoptotic cells after transfection with miR-27a mimics or inhibitors. G: qPCR analysis of plasticity-related gene expression (*SynCAM* and *PSD95*) following miR-27a modulation. H–I: Western blot analysis of SynCAM protein expression in neurons transfected with miR-27a mimics or inhibitors (n=3). Data are presented as mean±SEM. *: P<0.05；**: P<0.01； and ns: Not significant.

expression but did not significantly affect ATG5 protein levels (Figure 3F). The mimics also significantly increased the *BCL2*/*Bax* ratio and reduced *Caspase-1*, *Caspase-3*, and *Caspase-7* expression (Figure 3G, H). Caspase-3 protein levels tended to decrease after mimic treatment and increase after inhibitor treatment, although neither change was significant (Figure 3I, J). The mimics significantly reduced the mRNA and protein levels of the neuronal plasticity markers SynCAM and PSD95. Inhibition of miR-27a-3p tended to increase their expression, but the increases were not significant (Figure 3K–O). Collectively, these findings suggest that miR-27a-3p suppresses autophagy, apoptosis, and neuronal plasticity in SH-SY5Y cells.

miR-27a targets and regulates *PRKCA* expression

To further investigate the functional role of miR-27a, mRNA-seq was performed in primary porcine neural cells transfected with miR-27a mimics or mimic negative control (NC) (Figure 4A). Gene set enrichment analysis (GSEA) revealed significant enrichment of genes involved in axon guidance and dopaminergic synapses in the miR-27a mimic group, whereas

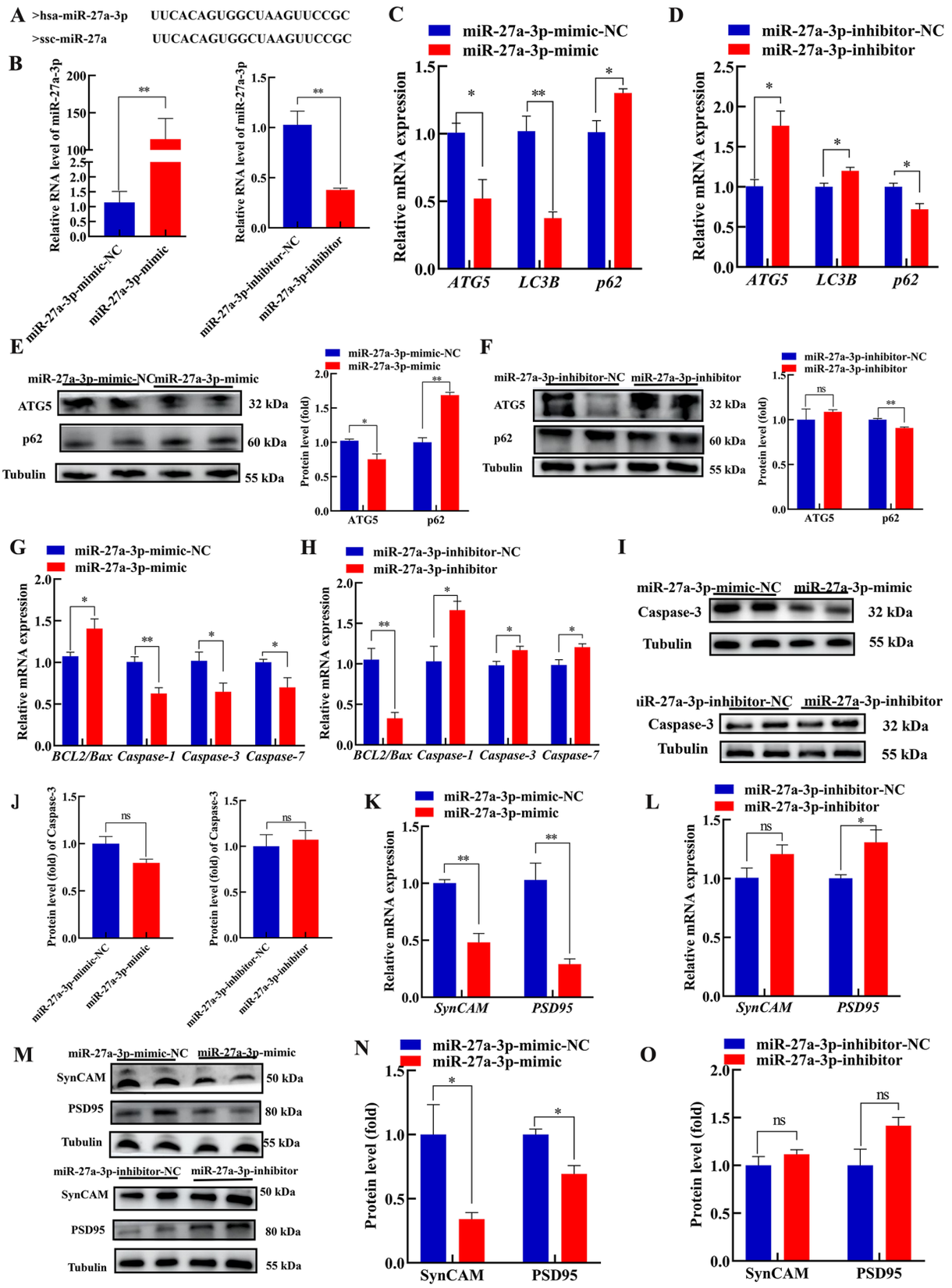

Figure 3 miR-27a-3p suppresses autophagy, apoptosis, and neuronal plasticity in SH-SY5Y cells

A: Sequence alignment showing complete identity between human hsa-miR-27a-3p and porcine ssc-miR-27a. B: qPCR validation of transfection efficiency for miR-27a-3p mimics and inhibitors in SH-SY5Y cells. C–D: Effects of miR-27a-3p mimics and inhibitors on mRNA expression of autophagy-related genes (*ATG5*, *LC3B*, and *p62*). E–F: Western blot analysis of ATG5 and p62 protein levels following transfection with miR-27a-3p mimics or inhibitors (n≥3). G–H: Expression levels of apoptosis-related genes (*BCL2*, *Bax*, *Caspase-1*, *Caspase-3*, *Caspase-7*) following miR-27a-3p modulation. I–J: Caspase-3 protein levels in response to miR-27a-3p mimics and inhibitors (n=3). K–L: Effects of miR-27a-3p mimics and inhibitors on mRNA expression of plasticity markers *SynCAM* and *PSD95*. M–O: Protein levels of SynCAM and PSD95 following miR-27a-3p mimic or inhibitor transfection (n=3). Data are presented as mean±SEM .*: P<0.05；**: P<0.01；and ns: Not significant.

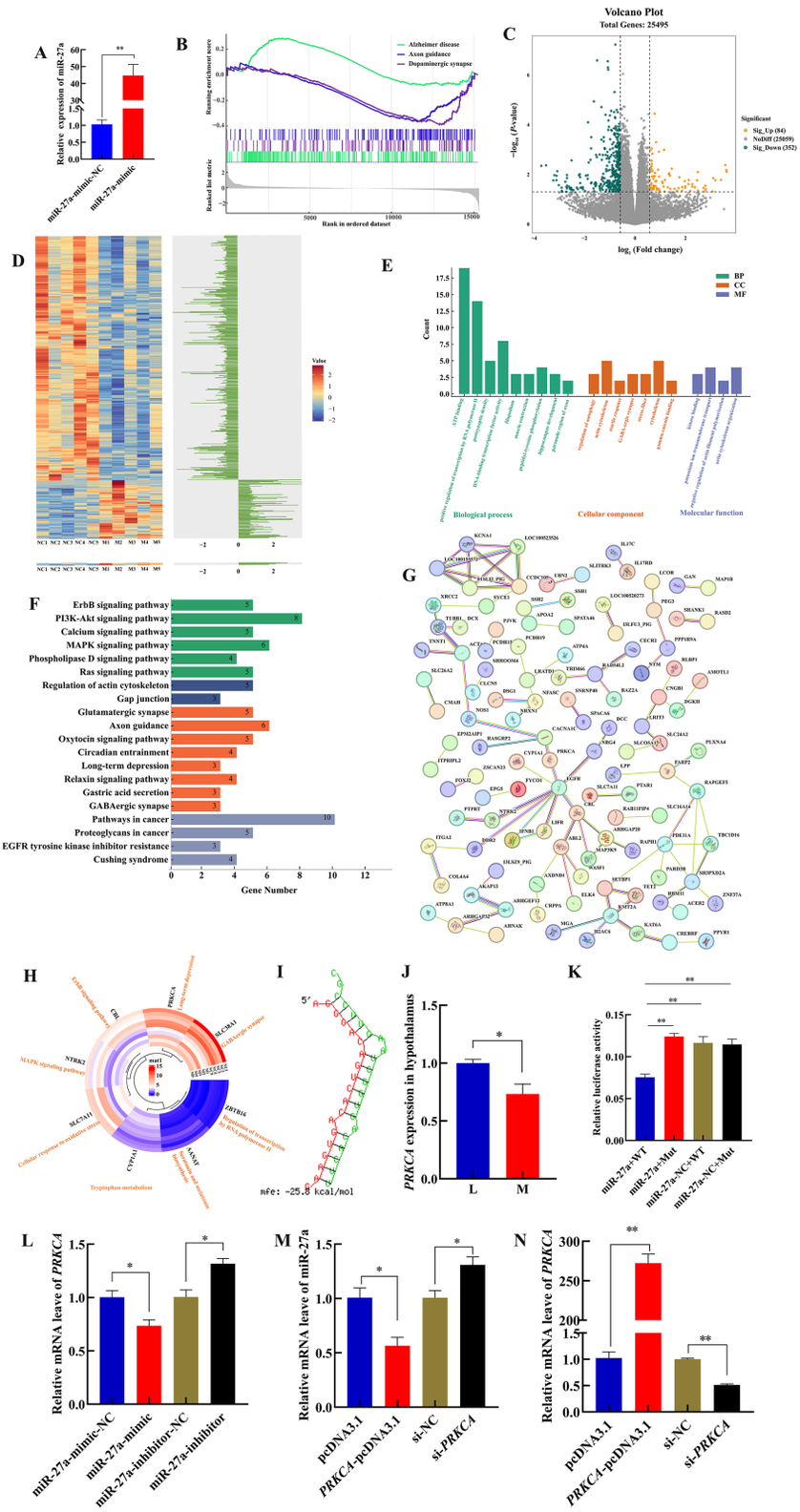

Figure 4 miR-27a targets and regulates *PRKCA* expression

A: Validation of miR-27a expression following transfection with miR-27a mimics in primary porcine neural cells. B: GSEA showing enrichment of pathways related to Alzheimer's disease, axon guidance, and dopaminergic synapses in the miR-27a mimic and mimic-NC groups. C–D: Volcano plot and heatmap illustrating DEGs between miR-27a mimic and mimic-NC groups. E–F: GO and KEGG enrichment analyses of DEGs. G: PPI network highlighting central hub genes among the DEGs. H: Heatmap of DEGs enriched in pathways related to amino acid metabolism, oxidative stress, and neural plasticity. I: Predicted binding interaction between miR-27a and the 3′-UTR of *PRKCA* using RNAhybrid. J: Relative expression of *PRKCA* in the hypothalamus of the most and the least aggressive pigs. K: Dual-luciferase reporter assay confirming direct targeting of *PRKCA* by miR-27a in porcine primary neural cells. L: Expression of *PRKCA* following transfection with miR-27a mimics or inhibitors. M: Validation of *PRKCA* overexpression and knockdown efficiency using *PRKCA*-pcDNA3.1 and si-*PRKCA*. N: miR-27a expression in response to *PRKCA* overexpression or knockdown. Data are presented as mean±SEM. *: $P<0.05$; **: $P<0.01$; and ns: Not significant.

Alzheimer disease-related genes were enriched in the NC group (Figure 4B). Using a threshold of $|\log_2(\text{fold change})| \geq 0.6$ and *P*-value<0.05, we identified 436 DEGs, including 84 upregulated and 352 downregulated genes (Figure 4C, D). GO and KEGG enrichment analyses indicated that these DEGs were significantly involved in ATP binding, transcriptional regulation by RNA polymerase II, DNA-binding transcription factor activity, cancer pathways, and the PI3K-Akt and MAPK signalling pathways (Figure 4E, F). Protein–protein interaction (PPI) analysis revealed that *EGFR*, *PDE11A*, and *RAD54L2* occupy central hub gene roles, with the node for EGFR demonstrating the most interconnected position within the network (Figure 4G). A total of eight genes were identified as being linked to key pathways, such as tryptophan metabolism, oxidative stress response, and long-term synaptic depression (Figure 4H), through the integration of GO, KEGG, and PPI data. Bioinformatic prediction indicated that miR-27a directly targets the 3′-UTR of *PRKCA* (Figure 4I), which was significantly downregulated in the hypothalamus of the most aggressive pigs (Figure 4J). This interaction was confirmed by dual-luciferase reporter assays (Figure 4K). The miR-27a mimics significantly reduced *PRKCA* expression, while its inhibitor enhanced it (Figure 4L). Furthermore, overexpression of *PRKCA* suppressed miR-27a levels, whereas siRNA-mediated knockdown of *PRKCA* increased miR-27a expression (Figure 4M, N). These results collectively demonstrate that miR-27a directly targets and regulates *PRKCA* expression.

PRKCA enhances autophagy, apoptosis, and plasticity in primary porcine nerve cells

To investigate the functional role of *PRKCA*, primary porcine neural cells were transfected with either a PRKCA overexpression vector (*PRKCA*-pcDNA3.1) or a targeted siRNA (si-*PRKCA*). Overexpression of *PRKCA* upregulated the expression of *ATG5* and significantly downregulated *p62* at both mRNA and protein levels (Figure 5A, C, D). In contrast, knockdown of *PRKCA* by siRNA led to decreased ATG5 and increased p62 expression (Figure 5B, C, E).

Apoptosis-related assays demonstrated that *PRKCA*-pcDNA3.1 significantly increased the mRNA expression of *Caspase-1*, *Caspase-3*, and *Caspase-7*, while reducing the *BCL2*/*Bax* ratio (Figure 5F, G). Flow cytometry further showed a significant increase in apoptotic cell populations following *PRKCA* overexpression, whereas si-*PRKCA* decreased apoptosis rates (Figure 5H, I). Protein analysis showed that Caspase-3 levels increased following PRKCA overexpression, although the change was not statistically significant. In contrast, inhibition of PRKCA expression led to a significant reduction in Caspase-3 levels (Figure 5J–L). Regarding neuronal plasticity, *PRKCA* overexpression enhanced the expression of *SynCAM* and *PSD95* at the mRNA level, whereas knockdown of *PRKCA* reduced their expression (Figure 5M). At the protein level, there was a significant impact on the expression of SynCAM (Figure 5J, K, N). Together, these results demonstrate that *PRKCA* promotes autophagy, apoptosis, and synaptic plasticity in primary porcine nerve cells.

miR-27a mitigates _PRKCA_-mediated autophagy, apoptosis, and synaptic plasticity in primary porcine nerve cells

Because miR-27a targets the 3′-UTR of *PRKCA*, we investigated whether miR-27a could counteract PRKCA-mediated effects in primary porcine neurons. Co-transfection of miR-27a mimics with either the empty vector (pcDNA3.1) or *PRKCA*-pcDNA3.1 significantly reduced *ATG5* mRNA expression (Figure 6A) and increased *p62* expression (Figure 6B). ATG5 protein levels were similarly reduced in both groups, with no significant difference between them (Figure 6C, G). The *BCL2*/*Bax* ratio increased in the miR-27a mimics+pcDNA3.1 group and was moderately elevated in the miR-27a mimics+*PRKCA* group (Figure 6D). Both co-transfection treatments also significantly reduced *Caspase-3* mRNA and protein levels (Figure 6E, F, H). Flow cytometry and TUNEL assays confirmed reduced apoptosis in both co-transfected groups, as indicated by lower apoptotic-cell proportions and weaker red fluorescence, respectively (Figure 6I–J; Supplementary Figure S2). Furthermore, miR-27a attenuated *PRKCA*-induced plasticity: *SynCAM* and *PSD95* mRNA (Figure 6K, L) and SynCAM protein levels (Figure 6M, N) were significantly reduced in both co-transfected groups. These findings demonstrate that miR-27a suppresses *PRKCA*-mediated autophagy, apoptosis, and synaptic plasticity in primary porcine neurons by directly targeting *PRKCA*.

mmu-miR-27a-3p modulates mouse behavior and impairs neuronal autophagy, apoptosis, and plasticity

Sequence alignment revealed that porcine miR-27a is identical to mouse mmu-miR-27a-3p (Supplementary Figure S3A). Bioinformatic analysis predicted that miR-27a-3p targets the 3′-UTR of mouse *PRKCA* (Supplementary Figure S3B). Subsequently, we randomly selected mice for the tube test (Supplementary Figure S3C). The results showed that mice with a higher winning rate exhibited increased expression of miR-27a-3p and decreased expression of *PRKCA* (Supplementary Figure S3D, E).

To investigate its functional role *in vivo*, miR-27a-3p mimics were injected into the hypothalamus of 28-day-old mice, and behavioral assays were conducted two days later (Figure 7A). In the open field test, mice receiving miR-27a-3p injections displayed a reduction in total movement distance and average speed. The time spent in the central area also showed a decreasing trend, although the difference was not statistically significant (Figure 7B–E; Supplementary Figure S3F). These results suggest that miR-27a-3p expression may be associated with a mild impairment of motor function. In the tube test, the miR-27a-3p mimics group showed a significantly lower winning rate (28%) compared to controls, indicating diminished social dominance (Figure 7F). Similarly, in the warm spot test, these mice spent significantly less time occupying the heat source (Figure 7G). Post-behavioral analyses revealed that hypothalamic injection of miR-27a-3p mimics significantly increased miR-27a-3p expression and suppressed *PRKCA* (Supplementary Figure S3G, H). Autophagy-related gene expression analysis showed downregulation of *ATG5* and *LC3B* and upregulation of *p62* (Figure 7H). Protein analyses confirmed decreased ATG5 and increased p62 levels (Figure 7I, J). Immunofluorescence staining showed reduced LC3B and elevated p62 signals (Figure 7K). Apoptosis-related changes included an increased *BCL2*/*Bax* ratio and reduced expression of *Caspase-3* and *Caspase-7* mRNA (Figure 7L). Protein levels of BCL2 were elevated, whereas Caspase-3 was decreased (Figure 7M, N). Corresponding immunofluorescence showed stronger BCL2 and weaker Bax signals (Figure 7O). Regarding neuroplasticity, expression of *CREB*, *SynCAM*, and *PSD95* was significantly reduced, both at the mRNA and protein

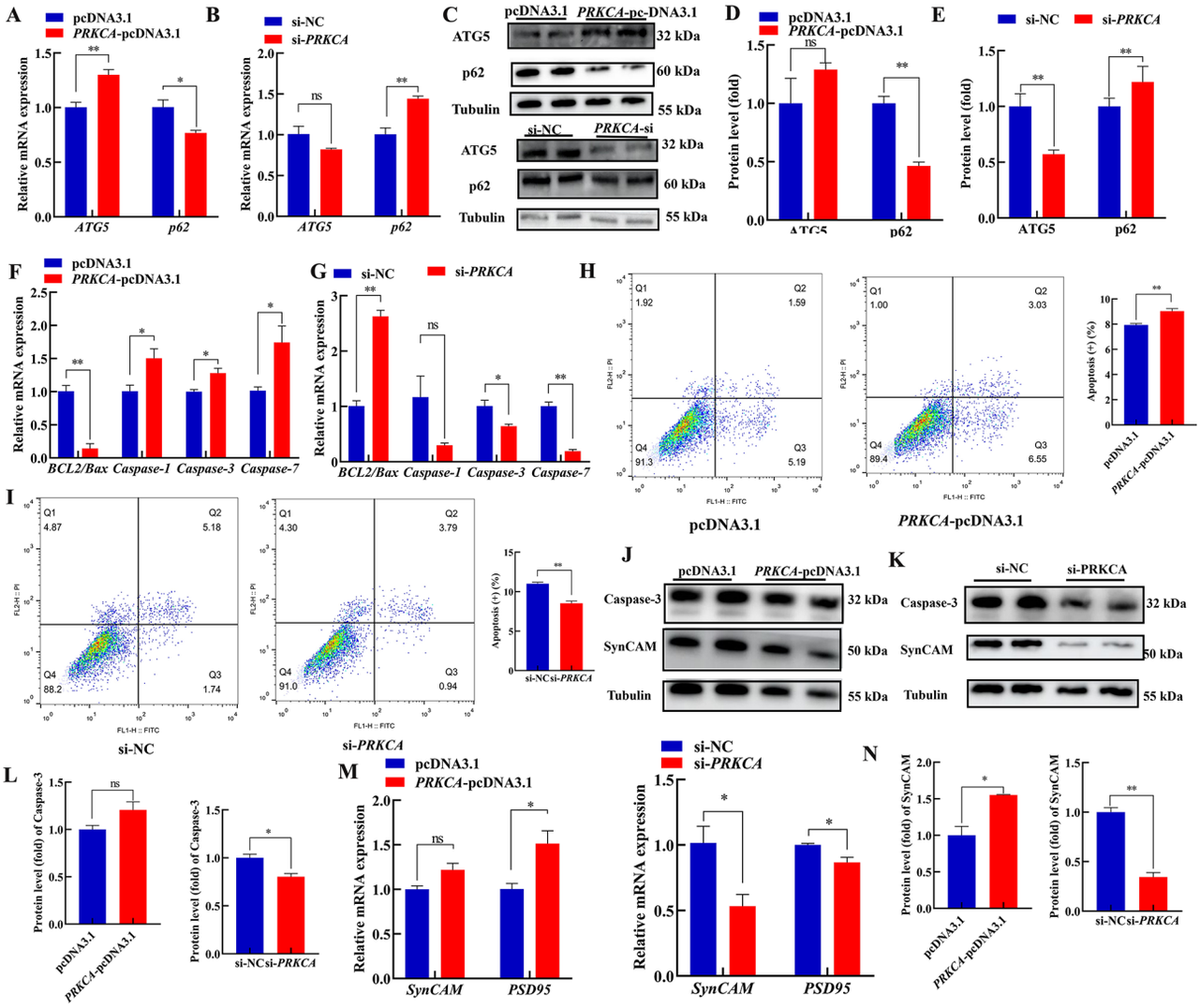

Figure 5 *PRKCA* regulates autophagy, apoptosis, and synaptic plasticity in primary porcine neurons

A–B: Relative mRNA expression levels of autophagy-related genes (*ATG5*, *p62*) following transfection with *PRKCA*-pcDNA3.1 or si-*PRKCA*. C–E: Protein expression levels of ATG5 and p62 in primary porcine nerve cells after PRKCA modulation (n=3). F–G: mRNA expression of apoptosis-related genes (*Bax*, *BCL2*, *Caspase-1*, *Caspase-3*, *Caspase-7*) in response to *PRKCA*-pcDNA3.1 or si-*PRKCA* treatment. H–I: Flow cytometry analysis of apoptosis rates in porcine neurons after *PRKCA* modulation. J–K: Western blot analysis of Caspase-3 and SynCAM protein expression following *PRKCA* overexpression or knockdown (n=3). L: Carried out statistical analysis on the protein expression of Caspase-3 in the J and K graphs. M: mRNA levels of plasticity-associated genes (*SynCAM*, *PSD95*) following *PRKCA*-pcDNA3.1 or si-*PRKCA* treatment. N: Carried out statistical analysis on the protein expression of SynCAM in the J and K graphs. Data are presented as mean±SEM. *: P<0.05； **: P<0.01； and ns: Not significant.

levels. Nissl staining revealed a decreased number of Nissl bodies in the miR-27a-3p-mimic group, suggesting impaired neuronal integrity (Figure 7P). At the protein level, the expression of SynCAM was significantly downregulated (Figure 7Q; Supplementary Figure S3I) and immunofluorescence staining showed reduced PSD95 signals (Figure 7R). Meanwhile, the results of the Nissl staining showed that after the injection of the miR-27a-3p mimics, the number of Nissl bodies decreased, indicating a reduction in the plasticity of neurons (Figure 7S). Collectively, these findings indicate that hypothalamic overexpression of mmu-miR-27a-3p reduced motor function, social competitiveness, and impaired autophagy, apoptosis regulation, and synaptic plasticity in mice.

DISCUSSION

Aggressive behavior helps animals secure resources, defend against threats, compete for territories or mates, and establish social dominance (Duarte & Zhang, 2023; Ischer et al., 2020). In intensive pig production, however, aggression is common and can cause injuries, stress, and economic losses. miRNAs are increasingly recognized as regulators of diverse biological processes, including behavior. In this study, hypothalamic miRNA sequencing of pigs with different aggression levels identified nine differentially expressed miRNAs associated with aggression. Notably, miR-27a was significantly upregulated in the most aggressive pigs.

Through a series of cellular and molecular experiments, we demonstrated that miR-27a inhibits autophagy, apoptosis, and plasticity in primary porcine nerve cells and SH-SY5Y neuroblastoma cells. Mechanistically, ssc-miR-27a directly targets the 3′-UTR of *PRKCA*, thereby modulating its expression and downstream pathways. This regulatory axis suppresses neuronal autophagy, apoptosis, and synaptic plasticity. Moreover, the murine homolog mmu-miR-27a-3p

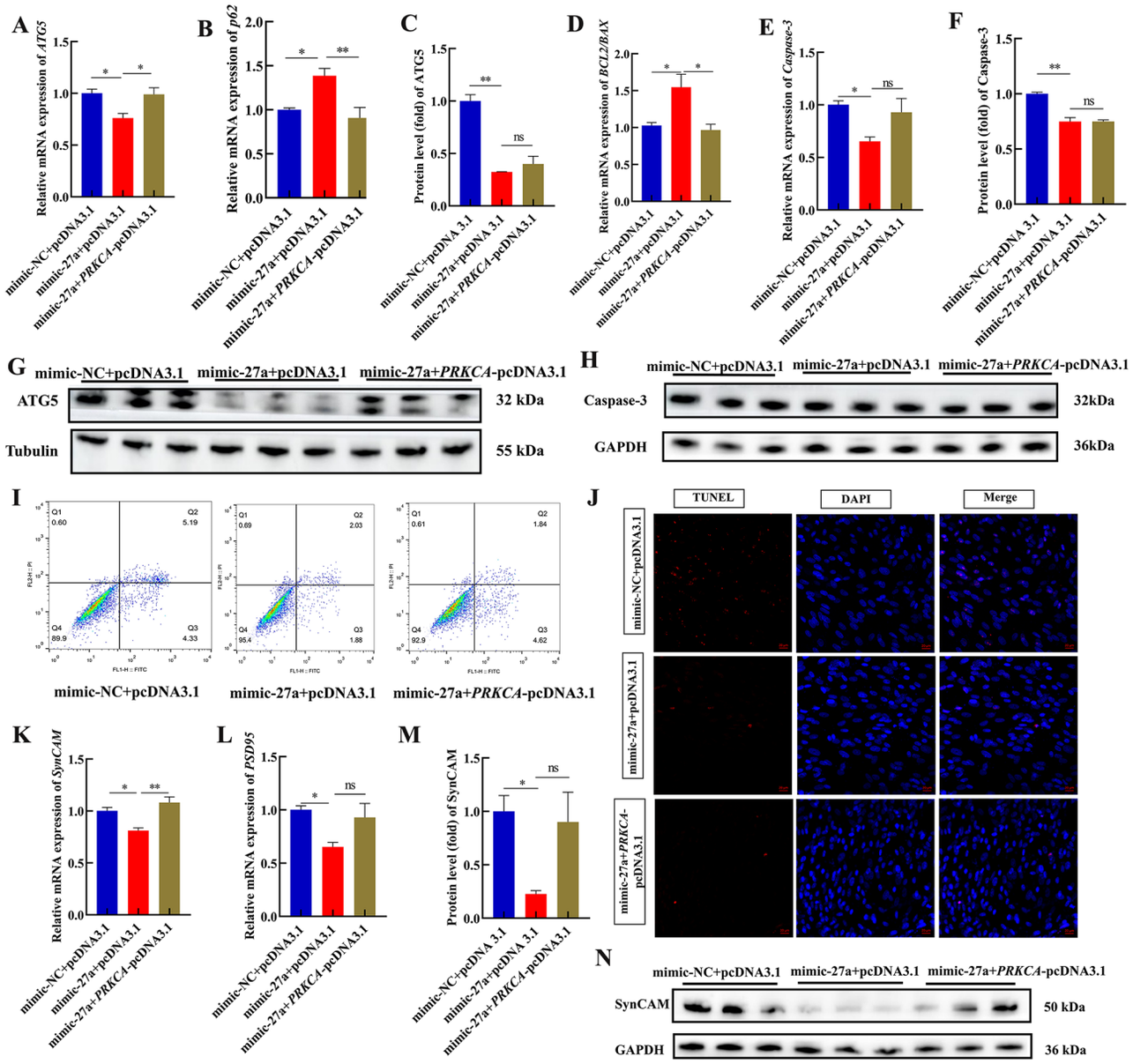

Figure 6 miR-27a attenuates PRKCA-induced autophagy, apoptosis, and synaptic plasticity in primary porcine nerve cells

A–B: mRNA expression levels of ATG5 and p62 in primary porcine nerve cells following co-transfection with mimic-NC+pcDNA3.1, miR-27a mimic+pcDNA3.1, or miR-27a mimic+*PRKCA*-pcDNA3.1. C, G: Protein levels of ATG5 under the same treatment conditions (*n*=3). D–E: mRNA expression levels of apoptosis-related genes (*Bax*, *BCL2*, and *Caspase-3*). F, H: Caspase-3 protein levels (*n*=3). I–J: Apoptosis was assessed by flow cytometry and TUNEL staining. The scale of the TUNEL staining is 20 μm. K–L: mRNA expression of plasticity-related genes SynCAM and PSD95. M–N: SynCAM protein expression (*n*=3). Data are presented as mean±SEM. *: $P<0.05$; **: $P<0.01$; and ns: Not significant.

was shown to reduce motor function in mice, reduce social dominance, and impair competitive performance. These behavioral changes were accompanied by marked inhibition of autophagy, apoptosis, and plasticity in mouse neurons.

Our findings are consistent with previous studies highlighting the role of miR-27a in neural stress responses. In a traumatic brain injury (TBI) model, miR-27a targets FoxO3a, reducing autophagy-related gene expression and ameliorating neurological deficits (Sun et al., 2017). Similarly, miR-27a-3p overexpression suppresses autophagy-related proteins and inflammasome activation, while promoting p62 accumulation. These results align with our observations in both primary porcine nerve cells and SH-SY5Y cells, where miR-27a downregulated *ATG5* and upregulated *p62*, indicating consistent suppression of autophagy (Li et al., 2020). In contrast, literature on the role of miR-27a in neuronal apoptosis is more heterogeneous. A previous study demonstrated that miR-27a-3p inhibition reduced apoptosis in an epilepsy model, as evidenced by increased *BCL2* and decreased *Bax* and *Caspase-3* (Lu et al., 2019). However, other studies reported that miR-27a/miR-27a-3p overexpression conferred neuroprotection by enhancing *BCL2* and suppressing pro-apoptotic markers such as *Bax* and *P53*. Our findings support the latter view: miR-27a overexpression elevated the *BCL2*/*Bax* ratio and reduced *Caspase-1*, *Caspase-3*, and *Caspase-7* expression. Conversely, miR-27a inhibition triggered the opposite effects. These molecular changes were corroborated by flow cytometry and TUNEL assays, which demonstrated a significant reduction in apoptotic cells upon miR-27a overexpression in porcine neurons (Cai et al., 2016; Moradi Vastegani et al., 2025).

An increasing body of evidence has highlighted a strong

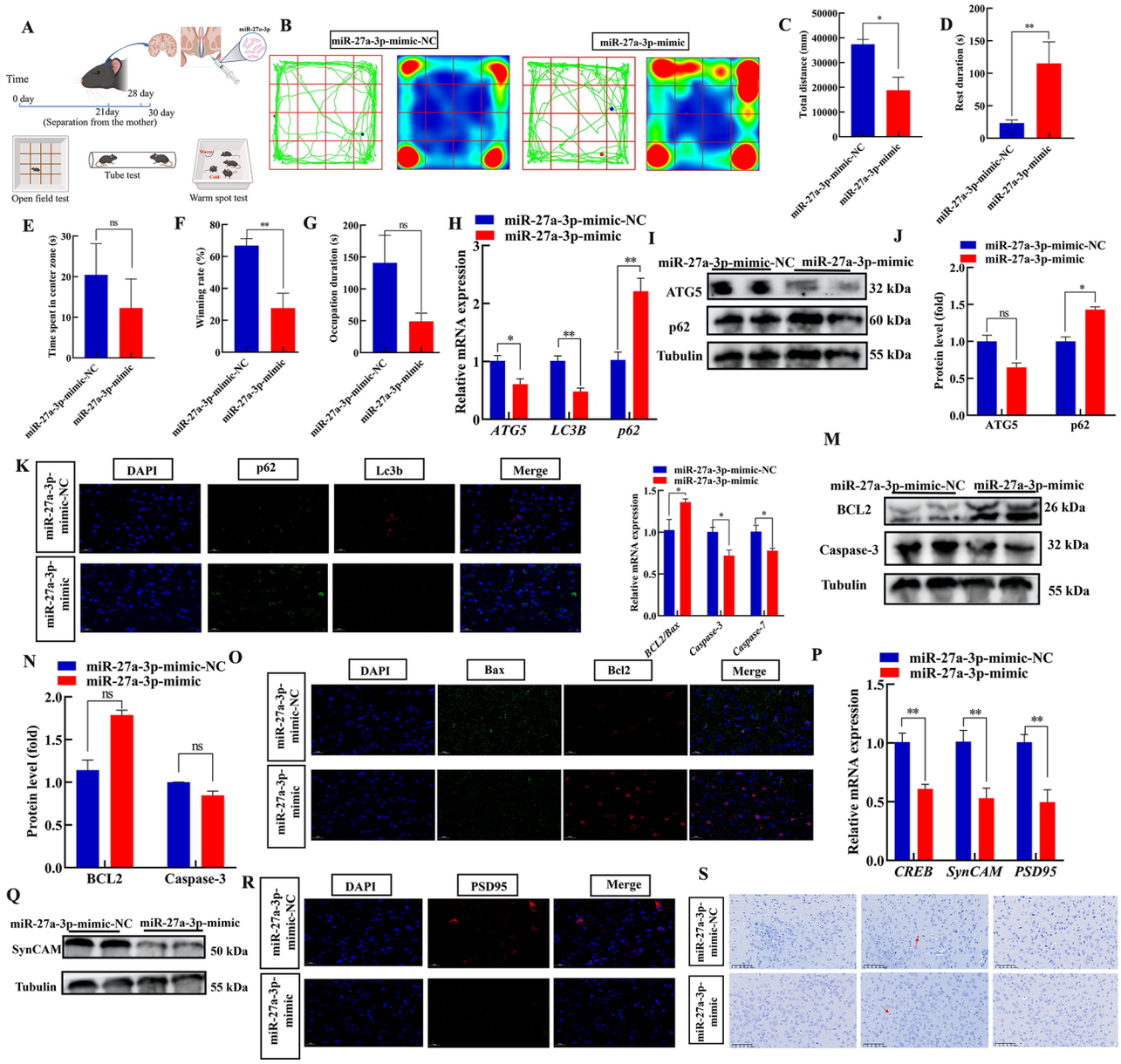

Figure 7 mmu-miR-27a-3p modulates mice behavior and inhibits neuronal autophagy, apoptosis, and plasticity

A: Schematic of hypothalamic injection of miR-27a-3p mimics or negative control (NC) into 28-day-old mice. B: Representative movement trajectories and time heatmaps from the open field test following injection. C–E: Quantification of total distance traveled, total resting time, and time spent in the central zone in the open field test. F: Winning rate in the tube test. G: Time spent on the heated spot in the warm spot test. H: Relative mRNA expression levels of *ATG5*, *LC3B*, and *p62* in brain tissue. I–J: Protein levels of ATG5 and p62 in brain tissue (n≥3). K: Immunofluorescence staining of p62 and LC3B in brain sections and the scale is 25 μm. L: mRNA expression levels of apoptosis-related genes (*Bax*, *BCL2*, *Caspase-3*, *Caspase-7*). M–N: Protein expression levels of BCL2 and Caspase-3 (n≥3). O: Immunofluorescence staining of Bax and BCL2 in brain sections and the scale is 25 μm. P: mRNA expression levels of plasticity-related genes (*CREB*, *SynCAM*, and *PSD95*). Q: Protein expression levels of SynCAM (n=3). R: Immunofluorescence staining of PSD95 in brain sections and the scale is 25 μm. S: Nissl staining of brain sections to assess changes in neuronal integrity. Scale bar: 100 μm. Data are presented as mean±SEM. *: P<0.05； **: P<0.01； and ns: Not significant.

correlation between *PRKCA* (Protein Kinase C Alpha) and emotional or neuropsychiatric disorders. In zebrafish with *PRKCA* deficiency, anxiety-like behavior, impaired social preference, and abnormal group interactions have been observed (Hu et al., 2023). Moreover, copy number variations (CNVs) in the *PRKCA* gene have been linked to autism spectrum disorder (ASD) (Turner et al., 2016). Functionally, *PRKCA* plays a central role in regulating apoptosis and autophagy. Importantly, apoptosis, autophagy, and synaptic plasticity of neurons are essential for maintaining stable behavioral patterns (He et al., 2023; Nixon & Rubinsztein, 2024; Shi et al., 2024). Its involvement in autophagy is context-dependent, with evidence supporting both stimulatory and inhibitory effects (Wang et al., 2017; Yu et al., 2022). For instance, activation of PKCα promotes TOCP-induced autophagy (Deng et al., 2020), while PKCα mediates palmitic acid-induced autophagic responses (Chen et al., 2019). In the present study, *PRKCA* overexpression led to increased mRNA and protein levels of *ATG5*, along with a reduction in *p62* protein levels—hallmarks of enhanced autophagic flux. These results are largely consistent with Deng et al.'s findings linking LC3 upregulation to autophagy activation. The observed discrepancy in p62 expression may reflect differences in cell type, stimulus, or the extent of autophagic induction (Deng

et al., 2020).

In relation to apoptosis, PKCα enhances TRAIL-induced apoptosis by phosphorylating *GSK3β* and upregulating *Caspase-3* (Gao et al., 2016). Consistent with this, we found that *PRKCA* overexpression significantly elevated Caspase-3 expression, supporting its pro-apoptotic role. Additionally, *PRKCA* is well-established as a critical regulator of neuronal plasticity. Upon synaptic stimulation, PKCα is rapidly activated in a process dependent on calcium influx via *NMDA* receptors and *BDNF* signaling (Colgan et al., 2018). Impaired PKCα signaling has been associated with deficits in neural development and synaptic plasticity (Barks et al., 2019). In agreement with these reports, our data show that *PRKCA* overexpression significantly upregulates synaptic plasticity markers *SynCAM* and *PSD95* in primary porcine nerve cells, suggesting that *PRKCA* promotes neuronal plasticity.

Following intrahypothalamic injection of miR-27a-3p in mice, neuronal apoptosis was markedly suppressed, consistent with the neuroprotective and anti-apoptotic effects of miR-27a-3p reported in a cerebral hemorrhage model (Xi et al., 2018). Mice receiving miR-27a-3p mimics also exhibited reduced motor function and a predominantly subordinate status.Reduced social dominance has been associated with diminished aggressive tendencies or capacity (Pavlova et al., 2024). This finding contrasts with the positive correlation between miR-27a expression and aggression observed in pigs. The divergence may reflect contextual differences: in pigs, elevated miR-27a expression during aggression may be a response to concurrent stress or environmental stimuli rather than a direct cause of aggression. By contrast, our murine model manipulated miR-27a-3p directly, thereby reducing the influence of these confounding factors.

Behavioral phenotypes are also shaped by the complex architecture and connectivity of neural circuits, which vary substantially among species. Homologous neurons may respond to similar stimuli across species yet regulate different behaviors because their circuit connections differ (Mizunami et al., 2015; Wang et al., 2025). Such structural variation may partly explain the species-specific behavioral outcomes observed here.

Syncam1, a key regulator of synaptic plasticity, promotes the formation and stabilization of excitatory synapses. Transgenic mice overexpressing Syncam1 exhibit approximately a threefold increase in excitatory synapse number compared with controls, whereas its deletion reduces synapse density (Robbins et al., 2010). In addition, Syncam1 accelerates synaptic maturation and enhances neuronal survival (Doengi et al., 2016). In this study, miR-27a downregulated Syncam expression in both primary porcine neurons and mouse brain tissue.

Interestingly, mice with higher winning rates had elevated miR-27a-3p expression, whereas exogenous miR-27a-3p suppressed aggression-related behaviors. Elevated miR-27a expression was also detected in aggressive pigs. These findings suggest a possible negative-feedback mechanism in which miR-27a moderates aggressive behavior after it is initiated. They also underscore the complexity of miRNA-behavior interactions and the need for further species-specific research. This study was limited primarily by the relatively small sequencing sample size. Larger cohorts are therefore needed to assess the generalizability of our findings. Direct manipulation of miR-27a in the porcine hypothalamus will also be required to test the proposed mechanism in pigs.

CONCLUSION

In conclusion, miR-27a is differentially expressed in the hypothalamus of pigs with distinct levels of aggression. Functional analyses demonstrated that ssc-miR-27a suppresses autophagy, apoptosis, and synaptic plasticity in primary porcine neurons, with similar effects observed for hsa-miR-27a-3p in the SH-SY5Y cell line. Mechanistically, miR-27a directly targets the 3′-UTR of *PRKCA*, thereby modulating key neuronal pathways. In mice, hypothalamic injection of mmu-miR-27a-3p also inhibited neuronal autophagy, apoptosis, and plasticity; however, it produced behavioral outcomes characterized by reduced motor function, social dominance, and diminished competitive ability. This apparent discrepancy—where miR-27a correlates positively with aggression in pigs but suppresses aggression-related behaviors in mice—may reflect species-specific differences in neural circuitry, as well as a potential negative feedback role of miR-27a in regulating excessive aggression in pigs. Collectively, these findings establish miR-27a/miR-27a-3p as a conserved regulator of neuronal processes while underscoring its context-dependent behavioral effects across species. Further investigation is warranted to determine whether miR-27a functions as a feedback mechanism to fine-tune aggressive behavior in pigs.

SUPPLEMENTARY DATA

Supplementary data to this article can be found online.

COMPETING INTERESTS

The authors declare that they have no competing interests.

AUTHORS' CONTRIBUTIONS

X.H.C. contributed to the study design, data analysis, and manuscript writing. C.L.Z., and H.Y. performed data analysis and reviewed the revised manuscript; Q.L.X., M.Z.L., J.H.C., and S.H.L. participated in the experiment and data analysis; Z.M.W., Y.D., H.W.B., W.G., J.H.F., M.J.Z., J.S.M., A.M., and M.M. were responsible for sample collection. B.Z. designed the entire study, revised the manuscript, and supervised its progress. All authors read and approved the final version of the manuscript.

REFERENCES

Alimohammadi I, Ahmadi Kanrash F, Abolaghasemi J, et al. 2018. Effect of chronic noise exposure on aggressive behavior of automotive industry workers. *The International Journal of Occupational and Environmental Medicine*, **9**(4): 170–175.

Aten S, Page CE, Kalidindi A, et al. 2019. miR-132/212 is induced by stress and its dysregulation triggers anxiety-related behavior. *Neuropharmacology*, **144**: 256–270.

Barks AK, Beeson MM, Matveeva T, et al. 2019. Perinatal ischemia alters global expression of synaptosomal proteins critical for neural plasticity in the developing mouse brain. *Developmental Neuroscience*, **40**(5-6): 638–650.

Burrows EL, Koyama L, May C, et al. 2020. Environmental enrichment modulates affiliative and aggressive social behaviour in the neuroligin-3 R451C mouse model of autism spectrum disorder. *Pharmacology Biochemistry and Behavior*, **195**: 172955.

Cai Q, Wang T, Yang WJ, et al. 2016. Protective mechanisms of microRNA-27a against oxygen-glucose deprivation-induced injuries in hippocampal neurons. *Neural Regeneration Research*, **11**(8): 1285–1292.

Chen P, Liu HD, Xiang H, et al. 2019. Palmitic acid-induced autophagy increases reactive oxygen species via the Ca^{2+}/PKCα/NOX4 pathway and impairs endothelial function in human umbilical vein endothelial cells. *Experimental and Therapeutic Medicine*, **17**(4): 2425–2432.

Coleman PT, Costanza-Chavez GW, Martin HN, et al. 2024. Prior

experience with behavioral control over stress facilitates social dominance. *Neurobiology of Stress*, **28**: 100597.

Colgan LA, Hu M, Misler JA, et al. 2018. PKCalpha integrates spatiotemporally distinct Ca(2+) and autocrine BDNF signaling to facilitate synaptic plasticity. *Nat Neurosci*, **21**: 1027–37.

Deng Q, Jiang L, Mao L, et al. 2020. The role of protein kinase C alpha in tri-ortho-cresyl phosphate-induced autophagy in human neuroblastoma SK-N-SH cells. *Journal of Applied Toxicology*, **40**(11): 1480–1490.

Desire S, Turner SP, D'Eath RB, et al. 2016. Prediction of reduction in aggressive behaviour of growing pigs using skin lesion traits as selection criteria. *Animal*, **10**(8): 1243–1253.

Doengi M, Krupp AJ, Körber N, et al. 2016. SynCAM 1 improves survival of adult-born neurons by accelerating synapse maturation. *Hippocampus*, **26**(3): 319–328.

Duarte B, Zhang J. 2023. The motive of competition but not courtship positively correlates with self-reported use of aggressive humor: a critical test of the contests- vs. mate-choice hypotheses. *Frontiers in Psychology*, **13**: 1056217.

Galli MC, Lagoda ME, Gottardo F, et al. 2023. The role of environmental enrichment and back fat depth in the intensity of aggressive behavior performed by sows during the establishment of the dominance hierarchy. *Animals*, **13**(5): 825.

Gao XJ, Xu FM, Zhang HT, et al. 2016. PKCα-GSK3β-NF-κB signaling pathway and the possible involvement of TRIM21 in TRAIL-induced apoptosis. *Biochemistry and Cell Biology*, **94**(3): 256–264.

Guo YL, Zhao J, Xu QL, et al. 2022. Identification of functional single nucleotide polymorphisms in the porcine *SLC6A4* gene associated with aggressive behavior in weaned pigs after mixing. *Journal of Animal Science*, **100**(5): skac131.

Hage S, Van Meijel B, Fluttert F, et al. 2009. Aggressive behaviour in adolescent psychiatric settings: what are risk factors, possible interventions and implications for nursing practice? A literature review. *Journal of Psychiatric and Mental Health Nursing*, **16**(7): 661–669.

He GH, Li Y, Deng H, et al. 2023. Advances in the study of cholinergic circuits in the central nervous system. *Annals of Clinical and Translational Neurology*, **10**(12): 2179–2191.

Hu H, Long Y, Song GL, et al. 2023. Dysfunction of Prkcaa links social behavior defects with disturbed circadian rhythm in zebrafish. *International Journal of Molecular Sciences*, **24**(4): 3849.

Ischer G, Zuberbühler K, Fedurek P. 2020. The relationship between food calling and agonistic behaviour in wild chimpanzees. *Behavioural Processes*, **178**: 104182.

Jiang MH, Gu YF, Cai JF, et al. 2021. MiR-186-5p dysregulation leads to depression-like behavior by de-repressing SERPINF1 in hippocampus. *Neuroscience*, **479**: 48–59.

Li B, Huang XY, Yang C, et al. 2022. miR-27a regulates sheep adipocyte differentiation by targeting *CPT1B* gene. *Animals*, **12**(1): 28.

Li HC, Lu CX, Yao WF, et al. 2020. Dexmedetomidine inhibits inflammatory response and autophagy through the circLrp1b/miR-27a-3p/Dram2 pathway in a rat model of traumatic brain injury. *Aging*, **12**(21): 21687–21705.

Li XW, Xu M, Ding L, et al. 2019. MiR-27a: a novel biomarker and potential therapeutic target in tumors. *Journal of Cancer*, **10**(12): 2836–2848.

Lu J, Zhou NN, Yang P, et al. 2019. MicroRNA-27a-3p downregulation inhibits inflammatory response and hippocampal neuronal cell apoptosis by upregulating mitogen-activated protein kinase 4 (MAP2K4) expression in epilepsy: *in vivo* and *in vitro* studies. *Medical Science Monitor*, **25**: 8499–8508.

Mikkola S, Salonen M, Puurunen J, et al. 2021. Aggressive behaviour is affected by demographic, environmental and behavioural factors in purebred dogs. *Scientific Reports*, **11**(1): 9433.

Mizunami M, Hamanaka Y, Nishino H. 2015. Toward elucidating diversity of neural mechanisms underlying insect learning. *Zoological Letters*, **1**(1): 8.

Moradi Vastegani Z, Ghaedi-Heidari R, Oroujalian A, et al. 2025. Manuscript title: unravelling the neuroprotective role of miR-27a-3p in the MAPK pathway in Parkinson's disease. *Metabolic Brain Disease*, **40**(3): 141.

Nieuwenhuis JG, Lepping P, Mulder CL, et al. 2022. Aggressive behaviour of psychiatric patients with mild and borderline intellectual disabilities in general mental health care. *PLoS One*, **17**(10): e0272502.

Nixon RA, Rubinsztein DC. 2024. Mechanisms of autophagy-lysosome dysfunction in neurodegenerative diseases. *Nature Reviews Molecular Cell Biology*, **25**(11): 926–946.

Noh K, Cho WH, Lee BH, et al. 2023. Cortical astrocytes modulate dominance behavior in male mice by regulating synaptic excitatory and inhibitory balance. *Nature Neuroscience*, **26**(9): 1541–1554.

Pavlova IV, Broshevitskaya ND, Potekhina AA, et al. 2024. The effect of chronic overcrowding on social behavior and expression of neuroinflammation-associated genes in rats. *Biochemistry (Moscow)*, **89**(9): 1582–1594.

Robbins EM, Krupp AJ, De Arce KP, et al. 2010. SynCAM 1 adhesion dynamically regulates synapse number and impacts plasticity and learning. *Neuron*, **68**(5): 894–906.

Salerno D, Peruzzi G, Giuseppe Rubens P, et al. 2024. miRNA-27a-3p is involved in the plasticity of differentiated hepatocytes. *Gene*, **913**: 148387.

Shen CY, Tong X, Chen RN, et al. 2020. Identifying blood-based biomarkers associated with aggression in weaned pigs after mixing. *Applied Animal Behaviour Science*, **224**: 104927.

Shi Y, Fang Q, Hu Y, et al. 2024. Melatonin ameliorates post-stroke cognitive impairment in mice by inhibiting excessive mitophagy. *Cells*, **13**(10): 872.

Shi ZM, Malki A, Abdel-Salam ASG, et al. 2020. Association between soft drink consumption and aggressive behaviour among a quarter million adolescents from 64 countries based on the global school-based student health survey (GSHS). *Nutrients*, **12**(3): 694.

Shultz SR, Taylor CJ, Aggio-Bruce R, et al. 2022. Decrease in plasma miR-27a and miR-221 after concussion in Australian football players. *Biomarker Insights*, **17**: 11772719221081318.

Sun LQ, Zhao MM, Wang Y, et al. 2017. Neuroprotective effects of miR-27a against traumatic brain injury via suppressing FoxO3a-mediated neuronal autophagy. *Biochemical and Biophysical Research Communications*, **482**(4): 1141–1147.

Tubert C, Lo Nostro F, Villafañe V, et al. 2012. Aggressive behavior and reproductive physiology in females of the social cichlid fish *Cichlasoma dimerus*. *Physiology & Behavior*, **106**(2): 193–200.

Turner SP, Roehe R, Mekkawy W, et al. 2008. Bayesian analysis of genetic associations of skin lesions and behavioural traits to identify genetic components of individual aggressiveness in pigs. *Behavior Genetics*, **38**(1): 67–75.

Turner TN, Hormozdiari F, Duyzend MH, et al. 2016. Genome sequencing of autism-affected families reveals disruption of putative noncoding regulatory DNA. *American Journal of Human Genetics*, **98**(1): 58–74.

van der Steen HAM, Schaeffer LR, De Jong H, et al. 1988. Aggressive behavior of sows at parturition. *Journal of Animal Science*, **66**(2): 271–279.

Wang F, Xu C, Reece EA, et al. 2017. Protein kinase C-alpha suppresses autophagy and induces neural tube defects via miR-129-2 in diabetic pregnancy. *Nature Communications*, **8**(1): 15182.

Wang YF, Cheng LQ, Li DY, et al. 2025. The Chimpanzee Brainnetome Atlas reveals distinct connectivity and gene expression profiles relative to humans. *The Innovation*, **6**(2): 100755.

Wei DY, Osakada T, Guo ZC, et al. 2023. A hypothalamic pathway that suppresses aggression toward superior opponents. *Nature Neuroscience*, **26**(5): 774–787.

Weltens I, Bak M, Verhagen S, et al. 2021. Aggression on the psychiatric ward: prevalence and risk factors. A systematic review of the literature.

PLoS One, **16**(10): e0258346.
Xi TY, Jin F, Zhu Y, et al. 2018. miR-27a-3p protects against blood-brain barrier disruption and brain injury after intracerebral hemorrhage by targeting endothelial aquaporin-11. *Journal of Biological Chemistry*, **293**(52): 20041–20050.
Xu QL, Zhao J, Guo YL, et al. 2022. A single-nucleotide polymorphism in the promoter of porcine *ARHGAP24* gene regulates aggressive behavior of weaned pigs after mixing by affecting the binding of transcription factor p53. *Frontiers in Cell and Developmental Biology*, **10**: 839583.
Yang H, Zhang CL, Chao XH, et al. 2024. A functional single nucleotide polymorphism in the 3' untranslated region of the porcine JARID2 gene is associated with aggressive behavior of weaned pigs after mixing. *International Journal of Molecular Sciences*, **25**(1): 27.
Yang YF, Lu WW, Ning M, et al. 2022. A functional SNP rs895819 on pre-miR-27a is associated with bipolar disorder by targeting NCAM1. *Communications Biology*, **5**(1): 309.
Yu Y, Liu B, Li XX, et al. 2022. ATF4/CEMIP/PKCα promotes anoikis resistance by enhancing protective autophagy in prostate cancer cells. *Cell Death & Disease*, **13**(1): 46.
Zhang CL, Liu MZ, Xu QL, et al. 2025. Unraveling the molecular basis of aggression in pigs through integrated transcriptomic and metabolomic analyses. *Animal Advances*, **2**(1): e017.
Zhang CL, Yang H, Xu QL, et al. 2023. Comprehensive genome and transcriptome analysis identifies SLCO3A1 associated with aggressive behavior in pigs. *Biomolecules*, **13**(9): 1381.
Zhou TT, Zhu H, Fan ZX, et al. 2017. History of winning remodels thalamo-PFC circuit to reinforce social dominance. *Science*, **357**(6347): 162–168.
Zilkha N, Chuartzman SG, Fishman R, et al. 2024. Maternal high-fat or low-protein diets promote autism-related behavior and altered social behavior within groups in offspring male mice. *Scientific Reports*, **14**(1): 19227.